EINSTEIN (e-Journal)
Jurnal Hasil Penelitian Bidang Fisika
Available online http://jurnal.unimed.ac.id/2012/index.php/einsten
e-issn: 2407 – 747x, p-issn 2338 – 1981

CALCULATION OF ELECTRONIC PROPERTIES AND MECHANICAL PROPERTIES OF CUBIC PHASE CH3NH(3)PbCl3 USING DENSITY FUNCTIONAL METHOD

Russell Ong and Junaina Sahputri Sagala
Department of Physics, Faculty of Science and Technology, Universitas Islam Negeri Sumatera Utara
rsslong@uinsu.ac.id
Submit: December 2024. Approved: January 2025. Published: February 2025.

ABSTRACT

Organic-inorganic hybrid halide perovskite-based solar cells such as CH3NH3PbCl3 are known to have many advantages such as low price, simple preparation process and high photoelectric conversion rate. Therefore, we performed theoretical calculations to determine the electronic properties and mechanical properties of $CH_3NH_{(3)}PbCl_3$material with space group p3m3 with bulk system in this study. Both properties are calculated by the Density Functional Theory (DFT) method through Quantum ESPRESSO software. The electronic properties discussed include electronic band structure, density of states (DOS) curve, and projected density of state s (PDOS) curve, while the mechanical properties include elasticity constant (Cij), limb modulus (B), Young's modulus (E), shear modulus (G), and Poisson's ratio (υ). To determine these properties, the optimum lattice constant must be achieved through optimization of k-points and cut-off kinetic energy. The results show that the value of the lattice gap is 2.49 eV, and C_{11}, C_{21}, C_{44}, limbal modulus, Young's modulus, shear modulus, and Poisson's ratio are 143.83 GPa, 21.22 GPa, 28.24 GPa, 62.09 GPa, 101.75 GPa, 41.47 GPa, and 0.23 GPa, respectively. This shows that the cubic phase CH3NH3PbCl3 waste material is mechanically stable which also has great potential as a perovskite semiconductor material.

Keywords: CH3NH3PbCl3, DFT, Quantum ESPRESSO, Band Gap Energy, Elastic Constant

INTRODUCTION

Solar energy is one of the most attractive renewable energy sources in Asia and a key energy source to address global warming and the energy crisis. This energy can be harnessed through solar cells that work by converting sunlight into electrical energy, giving solar cells great potential for development. Today, solar cells have experienced significant developments, such as the emergence of silicon-based solar cells, thin-film solar cells to dye-sensitized solar cells (DSSC) which are the third generation of solar cells (Sidik, Pitriana, & Aliah, 2024).

Organic material-based DSSCs produced successfully achieved 13% efficiency in 2013. However, these solar cells are not stable and efficient because the liquid electrolyte is prone to leakage. Therefore, scientists developed solid state-based solar cells to replace DSSCs. Perovskite solar cells belong to this class of solar cells. Their light-absorbing active materials are made from a combination of organic-inorganic hybrid perovskites with hybrid metals. The

development of perovskite solar cells has shown significant progress with the maximum efficiency reaching five times since its appearance in 2009. This shows the interest in understanding the constituents, optimization of forming materials, and mechanism of photovoltaic effects (Boix, Nonomura, Mathews, & Mhaisalkar, 2014).

Research on perovskite solar cells was first investigated by Kojima et al. (2009) using organic perovskite -inorganic metal halide materials $CH_3NH_3PbI_3$and $CH_3NH_3PbBr_3$. The efficiency was measured at 3.8% with the liquid electrolyte configuration. From the initial research above, it can be seen that the perovskite is $ABX_3$where A is an organic cation ($CH_3NH_3^+$), M is a metal cation (Pb^{2+}), and X is an anion from the halide group (I^- and Br^-). However, one can vary A, B, and X with group I inorganic cations, metal cations Sn^{2+}, and anions Cl^-/F^- (Afsari, Boochani, & Shirdel, 2019). In this study, we focused on the organic-inorganic hybrid halide perovskite material $CH_3NH_3PbCl_3$ considering that this perovskite has the advantages of low cost, simple solution process, and low preparation temperature. In addition, experimental results also show excellent optical and electrical properties in light-emitting diode and photodetector applications (Roknuzzaman et al., 2018).

Some theoretical calculation research is needed to improve the stability and efficiency of organic-inorganic hybrid halide perovskite solar cells. Many research studies have been conducted in the field of $CH_3NH_3PbCl_3$perovskite. Rikuyun (2021) calculated the electronic properties of $CH_3NH_3PbCl_3$and obtained an energy band gap of 2.8059 eV. This calculation uses the Quantum ESPRESSO (QE) program with Projected Augmented Wave (PAW) type pseudopotentials with the Generalized Gradient Approximation Perdew-Burke-Enzerhof exchange-correlation functional (GGA-PBE) (Rikuyun, 2021). Sarkar, et al. (2019) plotted the XRD graphs of pure $CH_3NH_3PbCl_3$perovskite, 10% indium doping, and 20% indium doping based on Philips X'Pert pro powder X-Ray diffractometer (XRD) scans. They used Cu Kα radiation (kα = 1.5406 Å) and the scanning angle was set from the range 10^0-60^0 (Sarkar, Mazumder, Tripathy, Baishnab, & Palai, 2019). Busipalli et al. (2018) computed the perovskites $CH_3NH_3PbCl_3$, $CH_3NH_3PbBr_3$, and CH3NH3PbI3 with cubic and tetragonal phases. The software used is Vienna Ab-initio Simulation Package (VASP). According to VASP calculations for the cubic phase, they obtained a band gap energy of 2.42 eV with different cubic lattice parameters (Busipalli, Nachimuthu, & Jiang, 2019).

Althoughthe study of electronic/structural properties of $CH_3NH_3PbCl_3$ perovskite has been investigated both experimentally and computationally, the study of mechanical properties has not been reported until now. Mechanical properties are very important in determining whether a perovskite is stable or not. Therefore, the study aimed to reveal the mechanical properties, namely elastic constant (Cij), limb modulus (B), shear modulus (G), Young's modulus (E) and Poisson's ratio (υ). Since there are no experimental values of mechanical properties to compare, we compared the X-ray diffractometer (XRD) simulation graphs, band gap energy values, and computed lattice constant values with various published literature. This study uses the QE program with the Density Functional Theory (DFT) approach. The type of pseudopotential used is Troullier-Martins Norm-Conserving (NC with GGA-PBE).

RESEARCH METHODS

Research Tools

The tools in this research consist of software and hardware. Software in the form of virtual box, QE, Visualization for Electronic and Structural Analysis (VESTA), gnuplot, Matrix Laboratory (MATLAB), notepad++, and adobe photoshop CS3, while hardware is a laptop that has an Intel(R) Core(TM) i3-6006U CPU @ 2.00GHz and 4.00 GB of RAM.

Material Modeling

Before starting the calculation of scf, nscf,

dos, the crystal structure of the material under study, namely the cubic phase $CH_3NH_{(3)}PbCl_3$perovskite, is modeled. The input script whose lattice constants have been optimized (see lattice constant optimization) according to vc-relax calculations will be simulated via the VESTA program. This is very important to test whether the perovskite crystal structure is correct or not. Figure 1 shows the visualization of cubic phase $CH_3NH_3PbCl_3$perovskite. Readers may compare with the image from the literature, namely Busipalli, et al. (2018).

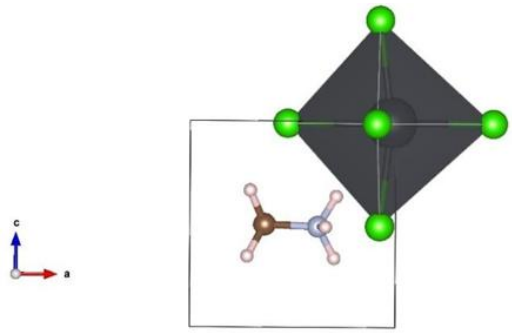

Figure 2. Crystal structure of CH3NH3PbCl3 Visualized with VESTA. (Brown: C; Blue: N; Light Pink: H; Gray: Lead; Green: Cl)

Calculation Parameters

Structure calculations were performed using the GGA PBE exchange-correlation function. The potentials between atomic nuclei and non-valence electrons are approximated using Troullier-Martins Norm- Conserving (NC) type pseudopotentials. The specific reason for choosing this type of pseudopotential is that some calculations only work with NC pseudopotentials, including: 1) Γ-point phonons; 2) third order energy derivatives; 3) non-resonance Raman; 4) anharmonic force constants (Hung, Nugraha, & Saito, 2022). Some other parameters are the cut-off kinetic energy for the wave function (ecutwfc), the cut-off kinetic energy for the charge density (ecutrho), k-points, and the optimized lattice constants.

RESULTS AND DISCUSSION

Convergence of Ecutwfc and K-points

To obtain the optimal ecutwfc value, ecutwfc was varied arbitrarily with a certain pattern. We start from ecutwfc = 15 Ry to 50 Ry with an increase of 5 Ry. The total energy of each ecutwfc is represented in Figure 2. Ecutwfc = 45 Ry is chosen as the optimal value because the convergence of the total energy is limited to an accuracy of 1 number behind the comma. This limitation was chosen considering that the program code for perovskite $CH_3NH_{(3)}PbCl_3$requires 12 atoms so that the scf calculation is reached in 391s. The more precise the total energy desired, the higher the ecutwfc required. However, the higher ecutwfc will lead to high time consumption for each calculation. If this is applied, the subsequent calculations (vc-relax, nscf, and bands) will take more time than the laptop can handle. The most important point is that the choice of ecutwfc value has passed the minimum ecutwfc value suggested by the pseudopotential data of each atom (Hung et al., 2022). Then, following Pitriana, et al. (2018) in determining ecutrho, namely ecutrho = 8 x ecutwfc (Pitriana, Wungu, Herman, & Hidayat, 2018), ecutrho = 360 Ry was obtained.)

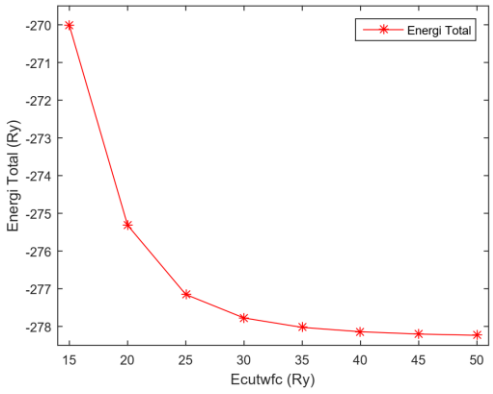

Figure 2. ecuwfc Convergence Chart

To obtain the optimal value of k-points, k-points are varied arbitrarily with a certain pattern. According to Wahyuni, et al. (2022), the general formula of k-points is n x n x n, so the determination of k-points starts from 1 x 1 x 1 grid (Wahyuni, 2022). The total energy of each ecutwfc is represented in Figure 3. 4 x 4 x 4 grid is chosen as the optimal value of k-points because the convergence of total energy is also limited to the accuracy of 1 number behind the comma. The main reason for choosing this limitation is that the output

data for perovskite $CH_3NH_3PbCl_3$requires 12 atoms so that the scf calculation requires 213 s. The calculation time becomes very long if the accuracy is increased. Unlike the ecutwfc convergence graph, the total energy convergence graph for the variation of k-points is not monotonically decreasing (Hung et al., 2022).

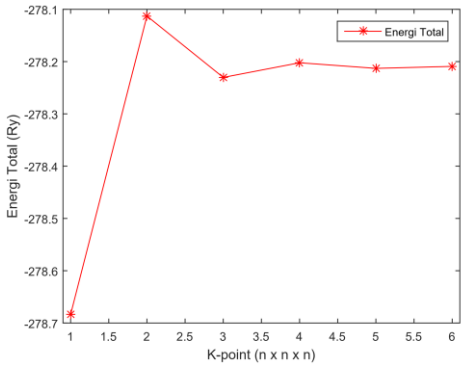

Figure 3. *k-points* Convergence Chart

Lattice Constant Optimization

The results of the calculation (comparison) of the lattice constant values of $CH_3NH_3PbCl_3$can be seen in table 1 and table 2.

Table 1. Calculation Results of Lattice Constant Values

$a_{initials}$ (Å)	$a_{relaxation}$ (Å)	Total Energy (eV)
5	5,447	-278,96484867
5,447	5,566	-279,06123645
5,566	5,589	-279,07948097
5,589	5,596	-279,08348759

Tabel 2. Comparison of Lattice Constants

Computational Result (Å)	Experiment Result (Å)	Percentage Error
5,596	5,68 (Poglitsch & Weber, 1987)	1,48 %
5,68 (Rikuyun, 2021)		0 %
a = 5,71, b = 5,69, dan c = 5,85 (Busipalli et al., 2019)		0,53 %, 0,18 %, dan 2,99 %

Table 1 shows that the value of the lattice constant after the last relaxation is 5.596 Å. The calculation of vc-relax was discontinued because the change between the lattice constant or total energy before and after relaxation was very small. In addition, the percentage error between the results of this study and the experimental results is also so small that the results obtained are scientifically acceptable. Hung, Nugraha and Saito (2022) stated that the typical error of using an exchange-correlation functional of the LDA or GGA type ranges from 1-2%.

The best results directly seem to belong to Rikuyun (2021). However, we find that the content of his thesis does not compute vc-relax calculations or other methods of finding balanced structures at all. We suspect that 5.68 Å was directly derived from experimental results by Poglitsch and Weber (1987). Conducting materials computing research based on this kind of DFT software is not appropriate. The reason is that no matter how small the threshold value of SCF convergence or the threshold value of ionic convergence of software calculations, the percentage error always exists. Furthermore, the computational results are compared with the results of Busipalli, Nachimuthu and Jiang (2019). Although both are computational results, there are some differences, such as software, exchange-correlation functional, or electronic convergence threshold value so that the value of the relaxation results of the two is different. both also have a percentage error where the comparison of the two shows the results of this study are slightly better.

XRD Graph Simulation

Using the optimal lattice constants from the previous discussion, the theoretical XRD graph is visualized using VESTA software as shown in Figure 4. For comparison, the reader can compare it with the experimental XRD graph of pure $CH_3NH_3PbCl_3$as well to compare the patterns (Sarkar, Mayengbam, Tripathy, & Baishnab, 2019). Although the 2θ angle from the literature is only limited to 60^0, a QE input file will be proven correct if the angle of maximum diffraction does not differ much from the experimental results. From Figure 4, we can see that the intensity spectra of the simulated XRD graph closely match the experimental XRD graph. For example, both the simulated and experimental results show

four intensity peaks between the angles of 25^0 to 30^0. Therefore, the QE input script is acceptable to be processed in the next calculation.

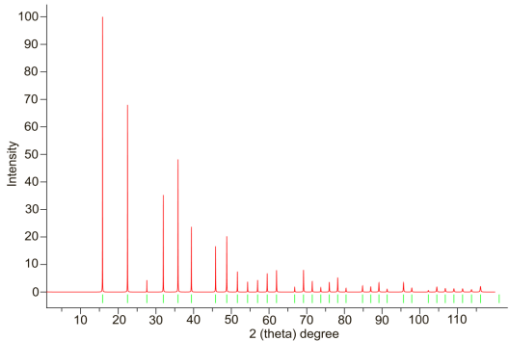

Figure 4. Visualization of XRD Graph of CH3NH3PbCl3 VESTA Output

Electronic Structure

From the electronic band structure shown in Figure 5, the left part shows the electronic band structure, while the right part shows the density of states.

It can be seen that there is a match between the electronic band curve and the density of states (DOS). The red arrow is the difference between the minimum energy of the conduction band and the maximum energy of the valence band, known as the direct band gap. It is called direct band gap because both the minimum point of the conduction band curve and the maximum point of the valence band curve fall on the same k-point, which is the point of symmetry R in the Brillouin zone.

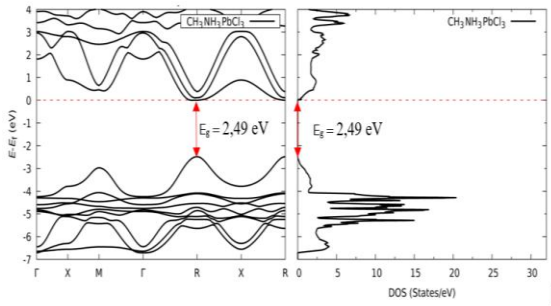

Figure 5. Electronic Band Structure and DOS of $CH_3NH_3PbCl_3$

Referring to the QE program output, a band gap value of 2.49 eV was obtained. Based on the results of the calculation gap energy obtained, then compared with the experimental gap energy as in table 3.

Tabel 3. Band Gap Energy Comparison

Computational Result (eV)	Ekperiment Result (eV)	Error Percentage
2,49		13,54 %
2,8059 (Rikuyun, 2021)	2,88 (Maculan et al., 2015)	2,57 %
2,42 (Busipalli et al., 2019)		15,97 %

The smallest percentage error seems to be obtained by Rikuyun (2021). However, the result is not scientifically reliable because the author directly quoted the lattice constant value from the experimental results. Another criticism of his results is that such a small percentage error does not make sense if the calculation uses the PBE exchange-correlation functional. It is common knowledge that DFT-based computations in general often produce band gap values that are much smaller than the original values. For this reason, additional corrections are needed, such as applying a hybrid functional, which will be a future work. We then compared the percentage error with the computational study by Busipalli, Nachimuthu and Jiang. (2019). They obtained 2.42 eV, so the largest percentage error is in their study. This may be the impact of obtaining the lattice constant c which is already slightly different from the experiment (percentage error 2.99%). In addition, the pseudopotential type was not mentioned at all in the contents of their journal. Thus, the best result is in our hands.

The DOS curve shown in Figure 5 on the right is basically the number of different states at a certain energy level that are allowed to be occupied by electrons without knowing which atoms play the most role in the formation of these states. To obtain this information, the PDOS (Projected Density of States) calculation is carried out. The PDOS graph of CH3NH3PbCl3 is shown in Figure 6 where the curves consist of atoms C-2s, C-2p, C-3d, C-4f, H-1s, H-2p, H-3d, H-4f, N-2s, N-2p, N-3d, N-4f, Pb-6s, Pb-6p, Pb-6d, Pb-5f, Cl-3s, Cl-3p, Cl-3d, and Cl-4f. Of all these orbitals, the Cl-3p orbital dominates the valence band construction, while the Pb-6p orbital dominates the conduction band

construction. From the electron configuration of the Pb atom, it is known that the 6p sub-skin is only filled with 2 electrons.

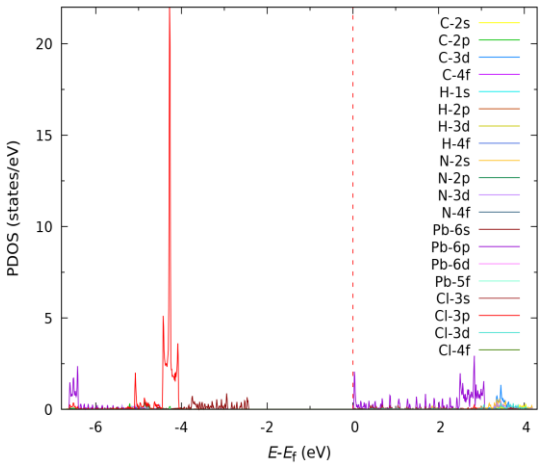

Figure 5. PDOS graph of CH3NH3PbCl3

Therefore, the Pb-6p orbital becomes empty because 2 electrons from Pb are transferred to Cl to form a bond between Pb2+ and Cl2- so that the Pb-6p orbital becomes the most dominant in the formation of DOS in the conduction band section. In contrast, the electron configuration of the Cl atom shows that the 3p sub-shell leaves only one electron and each Cl- anion becomes full with the transfer of electrons from the Pb2+ cation and $CH3NH_3^+$. Thus, the DOS forming part of the valence band is most dominantly formed by Cl-3p orbitals.

Mechanical Properties

After passing the lattice constant and electronic structure optimization calculations, the next step is to calculate the elasticity constant using QE. This stage only needs to run on the software when it has obtained stable geometry optimization results. After obtaining the elasticity constant results, it is necessary to review the stable conditions. This is done to ensure the validity of the calculations of B, G, E, and υ. In the analysis of elasticity constants using the QE program, each constant is obtained as follows.

Table 4. Results of Elasticity Constants

C_{ij} (Gpa)	$CH_3NH_3PbCl_3$
C_{11}	143,83
C_{12}	21,22
C_{44}	28,24
$C_{11} - C_{12}$	122,61
$C_{11} + 2C_{12}$	186,27

In accordance with the stability conditions, $C_{11} - C_{12} > 0$, $C_{11} + 2C_{12} > 0$, and $C_{44} > 0$ (Riaz et al., 2023), the results of the calculation of each constant indicate that most likely the cubic structure of CH3NH3PbCl3 is a stable material. If a material is unstable, then the B, E, G, and υ obtained will not be appropriate. Although there are no reference values to compare with Table 4, we are confident that the values obtained will be close to the experimental truth. The small percentage error in the lattice constants or the similarity of the XRD simulations to the experiments are the basis for our statement.

By substituting the values of C_{11}, C_{12}, and C_{44} into the formulas B, E, G, and υ (Bhandari, Zhang, & Yang, 2020), we will obtain the limbal modulus, Young's modulus, limbal modulus, and Poisson's ratio as shown in Table 5 below.

Table 5. Results of Elasticity Constants

Mechanical Properties	$CH_3NH_3PbCl_3$
B	62,09
E	101,75
G	41,47
υ	0,23

The above mechanical property values are also not compared with references as no literature is available to this extent.

CONCLUSIONS AND SUGGESTIONS

In conclusion of this research, we have conducted a computational study on cubic phase $CH_3NH_{(3)}PbCl_3$ perovskite using DFT calculation utilizing QE program. The optimized parameters are: ecuwfc = 45 Ry, ecutrho = 360 Ry, k-points = 4 x 4 x 4 grid, and lattice constant = 5.596 Å. Through these parameters, the XRD graph of VESTA simulation results is very similar to the experimental XRD graph where each intensity peak position occurs at the same 2 theta angle as the direct observation. Then, based on the DOS graph data / electronic band structure, the band gap energy of 2.49 eV is obtained. The PDOS graph then shows that

the Pb-6p orbitals dominate the formation of the conduction band structure, while the Cl-3p orbitals dominate the formation of the valence band structure. Finally, the elasticity constants of perovskite from QE evaluation are C_{11}= 143.83 GPa, C_{12}=21.22 GPa, and C_{44}= 28.24 GPa. Thus, this material is a stable material because it has met all stability criteria. If it is classified as unstable in terms of its elasticity constant, then the values of E, G, B, and υ obtained will be inappropriate. This research produces E, G, B, and υ as follows: 101.75 GPa, 41.47 GPa,62.09 GPa, and 0.23 GPa. This shows that the cubic phase $CH_3NH_3PbCl_3$perovskite material is mechanically stable which is also very potential as a perovskite semiconductor material.

Suggestions for future researchers are to explore thermal, optical and phonon properties using the same phase perovskite or to re-examine electronic/mechanical properties for tetragonal phase structures. In addition, the convergence accuracy limit of ecutwfc/k-points also needs to be improved to minimize the computational error.

REFERENCES

Afsari, M., Boochani, A., & Shirdel, F. (2019). Electronic and optical properties of two propounded compound in photovoltaic applications, CsPbI3 and CH3NH3PbI3: By Afsari, M.,

Boochani, A., & Shirdel, F. (2019). Electronic and optical properties of two propounded compound in photovoltaic applications, CsPbI3 and CH3NH3PbI3: By DFT. Optik, 199, 163360.

Bhandari, U., Zhang, C., & Yang, S. (2020). Mechanical and thermal properties of low-density Al20+xCr20-xMo20-yTi20V20+y Alloys. Crystals, 10(4).

Boix, P. P., Nonomura, K., Mathews, N., & Mhaisalkar, S. G. (2014). Current progress and future perspectives for organic/inorganic perovskite solar cells. Materials Today, 17(1), 16–23.

Busipalli, D. L., Nachimuthu, S., & Jiang, J. C. (2019). Theoretical Study on Halide and mixed halide Perovskite Solar Cells: Effects of Halide Atoms on the Stability and Electronic Properties. Journal of the Chinese Chemical Society, 66(6).

Hung, N. T., Nugraha, A. R. T., & Saito, R. (2022). Quantum ESPRESSO Course for Solid-State Physics. Jenny Stanford Publishing Pte. Ltd.

Maculan, G., Sheikh, A. D., Abdelhady, A. L., Saidaminov, M. I., Haque, M. A., Murali, B., … Bakr, O. M. (2015). CH3NH3PbCl3 Single Crystals: Inverse Temperature Crystallization and Visible-Blind UV-Photodetector. Journal of Physical Chemistry Letters, 6(19).

Pitriana, P., Wungu, T. D. K., Herman, H., & Hidayat, R. (2018). The Computation Parameters Optimizations for Electronic Structure Calculation of LiPbl3 Perovskite by the Density Functional Theory Method. IOP Conference Series: Materials Science and Engineering, 434, 012026.

Poglitsch, A., & Weber, D. (1987). Dynamic Disorder in Methylammoniumtrihalogenoplumbates (II) Observed by Millimeter-Wave Spectroscopy. The Journal of Chemical Physics, 87(11).

Riaz, M., Sahar, M. S. U., Ali, S. M., Shah, M. F., Zaidi, S. M. J., & Khan, M. I. (2023). Investigation of stress-induced effects on structural, optoelectronic, and elastic characteristics of cubic CaHfO3 perovskite oxide; A DFT study. Computational Condensed Matter, 37, e00846.

Rikuyun, N. R. (2021). Perhitungan Sifat Elektronik pada Fase Kubik CH3NH3BX3 (B = Pb dan Sn; X = Cl, I dan Br) dengan Mengunakan Metode Density Functional Theory. Universitas Islam Negeri Sunan Gunung Djati Bandung.

Roknuzzaman, M., Ostrikov, K. (Ken), Chandula Wasalathilake, K., Yan, C.,

Wang, H., & Tesfamichael, T. (2018). Insight into Lead-Free Organic-Inorganic Hybrid Perovskites for Photovoltaics and Optoelectronics: a First-Principles Study. Organic Electronics, 59, 99–106.

Sarkar, P., Mayengbam, R., Tripathy, S., & Baishnab, K. (2019). Cubic Methylammonium Lead Chloride Perovskite as a Transparent Conductor in Solar Cell applications: an Experimental and Theoretical Study. Indian Journal of Pure and Applied Physics, 57, 891–899.

Sarkar, P., Mazumder, J., Tripathy, S. K., Baishnab, K. L., & Palai, G. (2019). Structural, Optoelectronic, and Morphological Study of Indium-Doped Methylammonium Lead Chloride Perovskites. Applied Physics A: Materials Science and Processing, 125(8).

Sidik, A. R. F., Pitriana, P., & Aliah, H. (2024). Absorbance Optical Properties Calculation of ABX3 (A = Cs, Li; B = Pb; X = I, Br, Cl) Cubic Phase Using Density Functional Theory (DFT) Method. KnE Life Sciences, 8(1 SE-Articles).

Wahyuni, N. (2022). Studi Sifat Elektronik Pyrochlore Nd2Ir2O7 Menggunakan DFT. Jurnal Ilmu Dan Inovasi Fisika, 6(1), 61–71.